CHEMISTRY OF MATERIALS

Subscriber access provided by National Renewable Energy Laboratory Library

Article

Beyond Strain: Controlling the Surface Chemistry of CsPbI3 Nanocrystal Films for Improved Stability Against Ambient Reactive Oxygen Species

Taylor Moot, Desislava R. Dikova, Abhijit Hazarika, Tracy H. Schloemer, Severin N. Habisreutinger, Noemi Leick, Sean P Dunfield, Bryan A Rosales, Steven P. Harvey, Jason R. Pfeilsticker, Glenn Teeter, Lance M. Wheeler, Bryon W. Larson, and Joseph M. Luther

Chem. Mater., **Just Accepted Manuscript** • DOI: 10.1021/acs.chemmater.0c02543 • Publication Date (Web): 31 Aug 2020

is published by the American Chemical Society. 1155 Sixteenth Street N.W., Washington, DC 20036

Beyond Strain: Controlling the Surface Chemistry of $CsPbI_3$ Nanocrystal Films for Improved Stability Against Ambient Reactive Oxygen Species

Taylor Moot[1], Desislava R. Dikova[1,2], Abhijit Hazarika[1], Tracy H. Schloemer[1,3], Severin N. Habisreutinger[1], Noemi Leick[1], Sean P. Dunfield[1,4], Bryan A. Rosales[1], Steven P. Harvey[1], Jason R. Pfeilsticker[1], Glenn Teeter[1], Lance M. Wheeler[1], Bryon W. Larson,[1*] Joseph M. Luther[1*]

[1]*National Renewable Energy Laboratory, Golden, CO 80401, USA*
[2]*University of Michigan, Ann Arbor, MI 48109, USA*
[3]*Department of Chemistry, Colorado School of Mines, Golden, CO 80401 USA W*
[4]*Materials Science and Engineering Program, University of Colorado, Boulder, CO 80309, USA*
**Corresponding Authors: Bryon.Larson@NREL.gov, Joey.Luther@NREL.gov*

Abstract

Colloidal halide perovskite nanocrystals (NCs) have the possibility of easy scale-up due to their batch synthesis and have demonstrated excellent optoelectronic properties. In particular, perovskite NCs have remarkably high photoluminescence quantum yields in solution and as thin films and impressive open circuit voltages in photovoltaic devices. Despite these promising results, little work has been done to understand the stability of $CsPbI_3$ NCs for optoelectronic device applications. It has been previously shown that the ligands impart tensile surface strain which stabilizes the black 3D perovskite phase against phase degradation, making $CsPbI_3$ NCs some of the most structurally robust inorganic halide perovskites to date. However, understanding exactly how $CsPbI_3$ NCs degrade under ambient conditions is critical. We demonstrate that the degradation mechanism of NCs is unique from, and two orders of magnitude slower than, their polycrystalline thin film counterparts. Under specific conditions, $CsPbI_3$ NC films show a compositional instability instead of the phase instability seen in large grain $CsPbI_3$. This is mediated through reactions with superoxide and other reactive oxygen species which are initiated from surface defect states, O_2 and light. We then use this mechanistic insight to identify multiple strategies to prolong the lifetimes of $CsPbI_3$ NC films, by going beyond surface strain to mitigate key surface chemistries. We demonstrate that 1) minimizing the number of surface defects 2) using an alkylammonium bromide ligand surface treatment and 3) encapsulation with an oxygen scavenging layer all increase NC film lifetimes by inhibiting various steps in the photo-oxidation degradation reaction.

Introduction

Metal halide perovskite (ABX_3: A=methylammonium (MA), formamidinium (FA) or Cs^+; B=Pb^{2+} or Sn^{2+}; X=I^-, Br^-, Cl^-) nanocrystals are uniquely suited for deployment in large scale applications. First, perovskite nanocrystals (NCs) are crystallized in large batches during colloidal synthesis, removing the constraint of any preferential crystallization processes that are necessary during polycrystalline (PC, defined by grains >100 nm) perovskite thin film fabrication.[1–3] Second, perovskite NCs are processed using benign, green solvents such as octane, hexane or methyl

acetate (MeOAc) instead of dimethyl formamide (DMF) or dimethyl sulfoxide (DMSO), which are toxic and common solvents for thin-film deposition.[4] Combined, these two attributes allow for facile, substrate-independent, large-area deposition using scalable techniques, such as spray coating.[5] This enhances the utility of the well-known optoelectronic benefits of perovskite NCs including near-unity photoluminescence quantum yield and remarkably low open circuit voltage (V_{OC}) losses.[2,6–8] These properties have ignited interest into their use in light-emitting diodes (LEDs) and have led to the current record quantum dot (QD) solar cell with a certified power conversion efficiency (PCE) of 16.6%.[1,9–13]

Despite the promise of perovskite NCs, only a handful of studies have investigated their stability as high conductivity absorbers for photovoltaic (PV) applications. This is in contrast to the ample amount of progress in perovskite NC stability that has been achieved for LED application.[14–19] The majority of work for PV applications thus far has been on phase stability because α-$CsPbI_3$ (or an alternate 3D perovskite phase) is known to be metastable at room temperature, and $CsPbI_3$ NCs have shown improved phase stability over $CsPbI_3$ polycrystalline (PC) thin films due to their tensile surface strain.[1,20,21] Enhanced phase stability has recently lead to an uptick in research on PV device stability, through introducing doping (Yb^{2+}), modifying the surface ligands (phenyltrimethylammonium bromide; PTABr) and the device architecture itself.[5,6,11,22] For example, a recent report used SnO_2 as the electron transport material instead of the traditional TiO_2, reaching impressive perovskite NC device stabilities, akin to what has been shown for PC perovskite thin films.[12,23]

While these improvements in stability are critical to the success of perovskite NCs, there has been little to no work to understand the underlying degradation mechanisms of $CsPbI_3$ NCs and if or how this differs from PC film degradation. It has been shown that PC perovskite films typically degrade either through a compositional or phase instability when exposed to H_2O, O_2, heat and/or light.[24–34] For example, $MAPbI_3$ PC films are known to compositionally degrade into methylamine, HI and PbI_2, which can ultimately degrade to $PbCO_3$ and I_2 whereas $CsPbI_3$ PC films are phase unstable.[1,34,35] Without understanding the exact degradation pathway, it is difficult to systematically improve the stability of any active layer or ultimately an entire PV device.[36] For example, by determining that H_2O is a major degradation initiator for PC perovskite films, modifications to the device architecture aimed at minimizing water ingress through the use of hydrophobic surface treatments or contact layers resulted in 1000s of hours of device operational

stability.[37–39] Understanding the relevant degradation initiators in perovskite NCs can directly inform the selection of durable device components to improve device stability for optoelectronic devices such as PVs or LEDs.

Here, we deliberately expose $CsPbI_3$ NCs to controlled environmental atmospheric stressors (i.e. H_2O, O_2, light) with *in-situ* characterization to probe optical and structural properties of perovskite NCs and compare the results to $CsPbI_3$ PC films. We find that $CsPbI_3$ NCs undergo photo-oxidation initiated by superoxide ($O_2^{\bullet-}$) and other reactive oxygen species (ROS) that causes NC optical bleaching – distinct from phase changes found for bulk PC $CsPbI_3$. Thus, the materials degrade *via* completely different pathways, at different timescales and into different products despite having a similar composition, emphasizing the uniqueness of NCs. We then target ligand treatment strategies to mitigate superoxide and ROS interactions with the surface through the use of an alkylammonium bromide (ABr) salt surface ligand treatment. Similar effects are found using the oxygen scavenging triarylamine-based hole-transport material (HTM) spiro-OMeTAD, which is commonly used in PV applications, promoting the NC advantageous stability.

Results and Discussion

Photoinduced spectral bleaching of thin films. Perovskite NC films were prepared following previously published methods *via* spin-coating from octane and treated by immersion in a $Pb(NO_3)_2$/MeOAc solution to exchange surface-bound oleate (OA^-) for acetate (Ac^-), forming an Ac^-/OAm^+ (oleylammonium) surface, unless otherwise noted.[1,40] PC $CsPbI_3$ thin films were prepared following previously published methods using a MeOAc antisolvent.[41]

First, the optical properties of $CsPbI_3$ NCs and PC $CsPbI_3$ are probed while aging at low humidity (~20% RH) and under constant illumination. This was done via a custom-built *in-situ* optical characterization tool (*see methods section*) that tracks film absorption over time during continuous illumination under a halogen light source to enable long-term photostability studies. Absorptance spectra (**Figure 1**) are collected at constant time intervals as noted in the legend of the figure. Here, $t_{1/2}$ is defined as the time (in hours) it takes for the absorptance of the film just above the bandgap (E_g) edge to drop to 50% of the starting absorptance. The absorptance at 650 nm is completely bleached for PC $CsPbI_3$ films (**Figure 1A**) within an hour of ageing, with a $t_{1/2}$ of 0.17 hrs. The PC films maintain a strong yellow color (**Figure 1D**) due to the absorptance at ~450 nm. This color change is indicative of an α (black) to δ (yellow) phase transition which is

further confirmed by X-ray diffraction (XRD) (**Figure S1**), fully consistent with previous reports.[1,42] However, we do note that over prolonged periods of time, bleaching of PC films does occur (**Figure S2**). Conversely, $CsPbI_3$ NC films (**Figure 1B**) take hours longer for the E_g edge absorptance to completely bleach in the same ambient conditions (20% RH), with a $t_{1/2}$ of 14.7 hrs (86x that of the PC thin film), whereupon the films appear colorless (**Figure 1E**) due to the lack of an absorptance feature at ~450 nm. This lack of color suggests that the observed changes cannot be attributed to a δ phase transition nor formation of PbI_2, in stark contrast to the PC films.[24,42] We note that ageing in the dark significantly reduces the degradation rate of NC films (**Figure S3**).

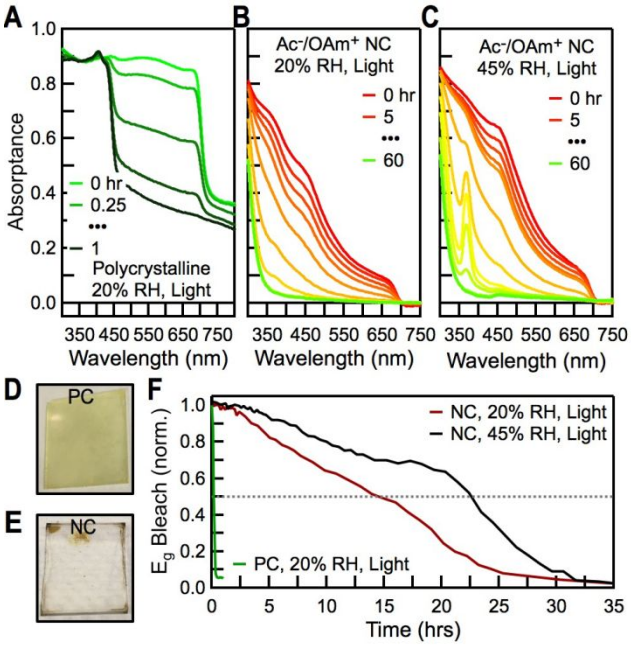

Figure 1: Ageing of PC and Ac^-/OAm^+ NC thin-films in ambient atmosphere. Absorptance spectra over time of **A**) PC films under illumination, 20% RH, **B**) NC films under illumination, 20% RH, **C**) NC under illumination, 45% RH. Each absorptance spectrum shown is taken at an equal time interval (hrs) until the last time point as noted in the legend. Photographs of an aged **D**) PC and **E**) NC film. **F**) Normalized E_g absorption bleach over time for PC (green) and NC films (red: low humidity, black: high humidity) under various ageing conditions.

H_2O is often cited as a degradation initiator for PC perovskite films, thus the NC films were studied under more humid conditions (45% RH) with illumination (**Figure 1C**).[19,23,37,39,43] Remarkably, the $t_{1/2}$ is 22.4 hrs, demonstrating that humidity does not exacerbate nor expedite NC degradation, although completely submerging NC films in H_2O does exacerbate degradation (**Figure S4**). Instead, degradation at higher humidity (45% RH) leads to the formation of an additional degradation product with an absorptance peak at ~370 nm which is attributed to

$Cs_4PbI_6 \cdot H_2O$,[44] even though this feature eventually disappears and the final absorptance spectrum is identical to that of NCs aged at a lower humidity. The bleaching rates just above the bandgap for PC films are compared to NC films in **Figure 1F**, validating that $CsPbI_3$ NC films degrade at a rate two orders of magnitude slower than their PC counterparts. The results indicate that while humidity does not further exacerbate NC degradation, the introduction of light does (**Figure S2**). The lack of effect of humidity on degradation rate is in contrast to what has been shown for $MAPbI_3$, where over the same humidity ranges the $t_{1/2}$ decreases by more than 50 percent.[29] We do note that the bleaching rate is slightly longer at elevated humidity and postulate that the formed intermediate, $Cs_4PbI_6 \cdot H_2O$, may slow down the bleaching reaction. Thus, we conclude that $CsPbI_3$ NCs films primarily undergo a photo-catalyzed degradation. The lack of phase change to δ-$CsPbI_3$ and the long $t_{1/2}$ both confirm that the ageing process of $CsPbI_3$ NCs is unique and markedly different than that of PC films, and as we will discuss, is heavily influenced by their unique surface chemistry.

Chemical, Structural, and Morphological Characterization. To further understand the chemical interactions associated with the spectral bleach, the fully aged colorless NC films were characterized in depth using a suite of morphological and analytical techniques. As we will show below, we can conclusively state that the ageing process for $CsPbI_3$ NCs results in 1) the loss of I, presumably as $I_{2(g)}$, 2) loss of N from oleylammonium (OAm^+) and 3) a photo-catalyzed reaction to form a Pb/Cs oxide and/or carbonate.

We first used XRD to identify any changes in the crystal structure (**Figure 2A**). The most prominent change is significant XRD peak broadening, which makes conclusive XRD analysis difficult. However, the XRD pattern of the aged NC films matches better with $PbCO_3 \cdot H_2O$ than with δ-$CsPbI_3$, particularly at higher angles. We note that the lack of phase change further supports arguments that there is ample surface strain in $CsPbI_3$ NCs to prevent significant phase degradation.[21] This suggests that the degradation, surprisingly, occurs *via* a compositional instability instead of a phase instability. Again, this is in stark contrast to what is seen for $CsPbI_3$ PC films. X-ray photoelectron spectroscopy (XPS) was then conducted to probe surface chemical and binding states of the fresh and degraded NC films. All XPS core level peaks (**Figure 2B-G**) as well as the VBM (**Figure S5**) of the aged NC films show a substantial shift to a higher binding energy, which signifies an increase in the difference between the valence band maximum and Fermi level of the material, plausibly due to a bandgap increase. The aged samples show broader

full width half maximum Cs 3d (**Figure 2B**) and Pb 4f (**Figure 2C**) core level peaks, representative of multiple chemical binding/electronic environments. Most notably, the I 3d peak (**Figure 2D**) and the N 1s peak (**Figure 2F**) completely disappear after ageing and an O 1s peak (**Figure 2E**) emerges. The loss of the N 1s signal from the oleylammonium (OAm^+) ligand is further confirmed by the disappearance of the ν_{NH3+} peak at 3150 cm^{-1} in the Fourier transform infrared spectroscopy (FTIR) spectrum (**Figure S6**). The main O 1s peak at 532.3 eV is attributed to a carbon-oxygen (C-O) bond, as is the 286.6 eV peak in the C 1s spectra (**Figure 2G**). The additional shoulder at ~530.6 eV in the O 1s spectra is due to a metal-oxygen (M-O) bond. This is further confirmed by the shift in the FTIR ν_{COO-} peak from 1560 cm^{-1} to ~1600 cm^{-1}, which occurs when a carboxyl group switches from being bound to a carbon, as it is as a ligand, to a metal (**Figure S7**) as well as the XRD (**Figure 2A**) that suggests $PbCO_3 \bullet H_2O$ is the degradation product.[45] $MAPbI_3$ PC films have been shown to degrade to $PbCO_3$ under similar ambient conditions.[34] We also note that over prolonged periods of time, PC $CsPbI_3$ also bleaches (**Figure S2**). Overall, it appears that there are iodine and nitrogen losses at the NC surface concomitant with oxygen growth, while the chemical environments of cesium, lead, and carbon significantly change over the course of ageing.

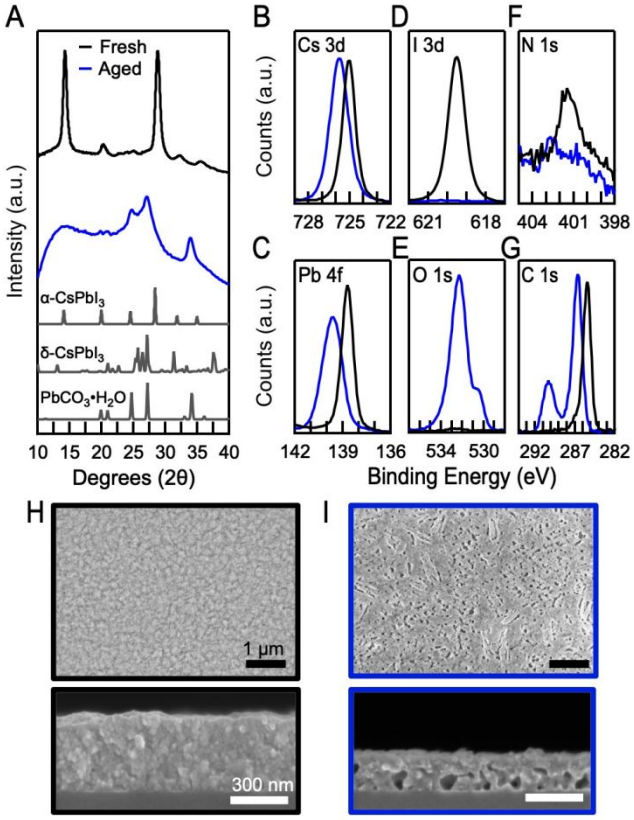

Figure 2: Structure and morphology characterization of a fresh (black) and fully degraded (blue) Ac^- /OAm^+ NC film. **A**) XRD with relevant standard patterns (grey). XPS spectra of **B**) Cs 3d, **C**) Pb 4f, **D**) I

3d, **E**) O 1s, **F**) N 1s, **G**) C 1s. Representative SEM images of a **H**) fresh **(**top down and cross section) and an **I**) aged (top down and cross section) thick, 4 layer, Ac^-/OAm^+ NC film.

As a result of chemical and structural changes of the NCs during ageing, the morphology of the material also changes; **Figures 2H** and **2I** show scanning electron microscopy (SEM) images of fresh and aged NC films, respectively. After ageing, rod-like features and large voids are evident throughout the NC film, which coincides with a significant loss in film thickness by ~45% shown in the SEM cross-sectional images (**Figure S8**). These observations align with the compositional changes we observe. For instance, the growth of rod-like morphologies has been seen when PC $MAPbI_3$ films degraded into $MA_4PbI_6{\cdot}2H_2O$, and the formation of voids has previously been reported for PC perovskite films and is attributed to the loss of volatile degradation products, namely $I_{2(g)}$.[29,46] The reduction in film thickness also matches well with the loss in crystal structure volume when transitioning from the black 3D perovskite γ-phase $CsPbI_3$ to Pb/Cs carbonates.[21,42,47]

Photoinduced ROS-mediated NC Degradation Mechanism. Undercoordinated sites on any perovskite surface have been theoretically and experimentally identified as key regions of the structure where degradation or passivation processes can occur.[35,46,48–50] It has been shown for PC $MAPbI_3$ films that O_2 preferentially localizes at these sites, where photoinduced electrons can also be trapped, leading to generation of superoxide ($O_2^{\bullet-}$) by electron transfer from the conduction band of the perovskite to O_2.[26,35,48,49,51–53] In perovskite NCs, the existence of some under-coordinated surface sites is likely caused by an imperfect ligand exchange of oleate for acetate.[26,54–56] Thus, we propose the following photo-oxidation degradation mechanism for $CsPbI_3$ NCs based on existing literature, experimental support and plausible intermediate reactions (**Figure 3)**:

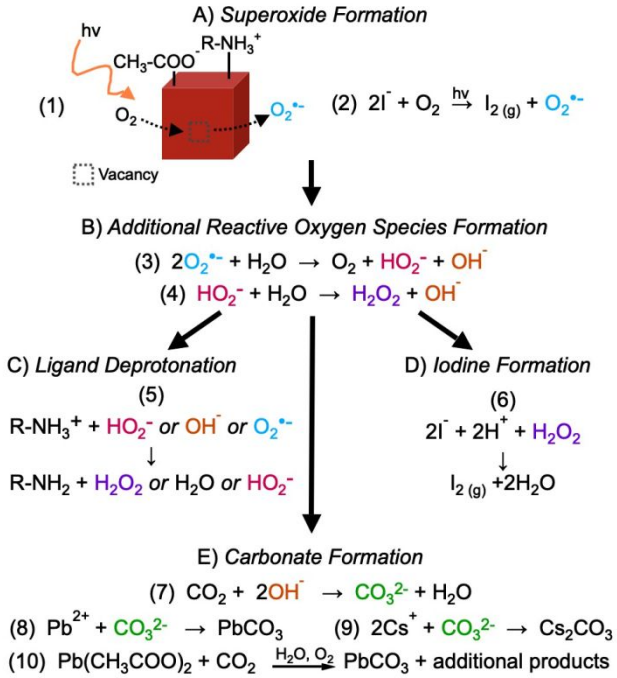

Figure 3: Proposed $CsPbI_3$ NC photo-oxidation mechanism. **A**) $O_2^{\bullet-}$ is formed either by photoinduced electron transfer from the NC to adsorbed O_2 in an I vacancy or during the formation of $I_{2\,(g)}$ from two interstitial I^-. **B**) $O_2^{\bullet-}$ can then react with H_2O to form additional reactive oxygen species (ROS). These ROS C) readily deprotonate oleylammonium, **D**) can further drive $I_{2\,(g)}$ formation and **E**) cause the formation of Pb/Cs carbonate species.[57]

First, we mention that in this case the electron involved in reducing molecular oxygen comes from photoexcitation, as has been shown for Pb based perovskites, which is entirely different from oxidation of the metal atom in the lattice that others have observed for tin-based perovskites in the dark.[58,59] **Figure 3A** shows two routes to $O_2^{\bullet-}$ formation at the NC surface: (1) reduction of adsorbed O_2 at vacancy sites as discussed above, and (2) light-induced formation of $I_{2(g)}$ from interstitial I^- ligands.[50] This is often shown to dominate for PC perovskites. Once $O_2^{\bullet-}$ is formed through either route, it could then react with H_2O and form additional ROS such as perhydroxyl (HO_2^-), hydroxide (OH^-), and hydrogen peroxide (H_2O_2) (**Figure 3B,** eq **3**, **4**) under illumination.[60,61] These ROS then initiate a cascade of self-propagating reactions, which on short timescales have shown to be beneficial.[62–64] But, over longer timescales, radical ROS can degrade the organic ligands by deprotonating oleylammonium ($R\text{-}NH_3^+$) to form oleylamine ($R\text{-}NH_2$) and additional ROS or H_2O and leave an undercoordinated I^- surface site (**Figure 3C,** eq **5**).[35,65,66] Additionally, hydrogen peroxide, with H^+ available from a deprotonated $R\text{-}NH_3^+$, is well known to cause I^- to react, forming $I_{2\,(g)}$ (**Figure 3D,** eq **6**), again leaving behind under-coordinated Pb sites.[61] The loss of $I_{2(g)}$ vapor has been shown to be a significant component of PC perovskite

degradation because the resulting under-coordinated Pb sites will continue to self-propagate degradation through the formation of more superoxide and other ROS.[27,45,67,68] Finally, the hydroxide can react with CO_2 and form carbonate (CO_3^{2-}) and H_2O (**Figure 3E,** eq **7**). CO_3^{2-} can then react with under-coordinated Pb^{2+} and Cs^+ sites to form a Pb- or Cs-carbonate species (**Figure 3E,** eq **8, 9**).[34] It is also possible that the surface Pb-Ac^- directly reacts with CO_2 to form $PbCO_3$ (**Figure 3E,** eq **10**).[57] While it is not necessary to have some molecular H_2O present for PC perovskites to degrade *via* methylamine and/or I_2 evolution, to the best of our knowledge, carbonate species cannot form without some available hydroxyl or water species.[34,57] We also note that most perovskite degradation mechanism studies stop at a degradation to PbI_2 and do not continue to the $PbCO_3$ formation, plausibly because upon degradation to PbI_2 the perovskite is already photo-inactive.[24,26,27,34,35] Here PbI_2 is not formed because this reaction requires the evolution of volatile A-site cation degradation products and Cs is not volatile.[35] Each reaction either forms an additional ROS, H_2O or leaves an under-coordinated site that will continue to propagate degradation of the NC. We emphasize that once superoxide has formed, these reactions require only one H_2O molecule to be present to propagate the formation of other ROS, after which H_2O is a by-product that further feeds a cascade of degradation reactions. Thus, while the existence of a few H_2O molecules is critical for this proposed degradation reaction to occur, a large increase in humidity will not further expedite degradation.

Photoinduced Spectral Bleaching of Multi-layer NC films. The proposed photooxidation degradation mechanism understood thus far focuses on the photooxidation of a single layer (~40 nm) of perovskite NCs, but it is unclear how this degradation mechanism applies to a thick NC film used in solar cells. In typical perovskite NC solar cell fabrication, multiple NC layers are consecutively deposited to build the solar cell active material.[1,10,11] Each layer adds a film of NCs ~ 50 nm thick. To investigate the thickness dependence of the proposed degradation mechanism, NC films with 2 layers (2L, ~100 nm thick, **Figure 4A**), 3 layers (3L, ~150 nm thick, **Figure 4B**), and 4 layers (4L, ~ 200 nm thick, **Figure 4C**) were aged under illumination and humid (~45% RH) conditions. Similar to the 1 layer thick films (**Figure 1C**), the spectra for multilayer films also show the signature photobleaching of the intermediate $Cs_4PbI_6{\cdot}H_2O$ at ~370 nm.[44] In the thickest NC films (3L and 4L), there is an additional intermediate peak at ~415 nm, which is likely the formation of a 2D layer, potentially from the acetate (Ac^-) ligand, and not δ-$CsPbI_3$.[1,69]

There is an increase in absorptance above the E_g at 800 nm due to enhanced diffuse scattering associated with the aforementioned morphological changes in the NC film (**Figure 2H, I**).

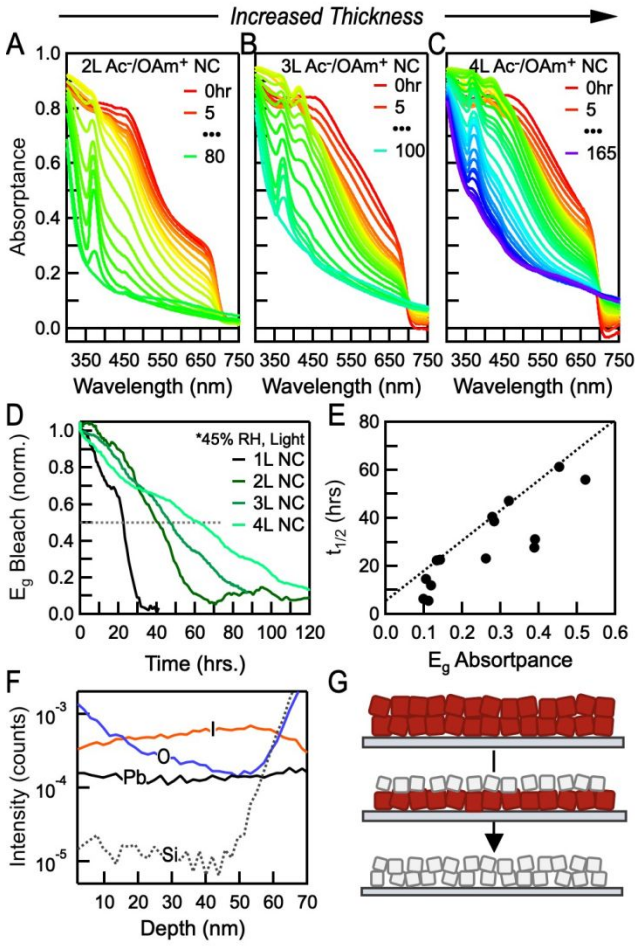

Figure 4: Absorptance spectra over time for ageing times of varying thickness Ac^-/OAm^+ NC films under illumination at 45% RH for **A**) 2 layers, **B**) 3 layers and **C**) 4 layers of QDs. Each absorptance spectrum shown is taken at an equal time interval (hrs) until the last time point as noted in the legend. **D**) Normalized E_g absorption bleach over time for Ac^-/OAm^+ NC films with 1-4 layers under illumination at 45% RH. **E**) $t_{1/2}$ lifetimes of $CsPbI_3$ Ac^-/OAm^+ NC films as compared to starting film E_g absorptance. The dashed line has the equation: $y=125.8x+5.5$. **F**) ToF-SIMS of a partially (55%) degraded $CsPbI_3$ QD film on glass probing the composition. **G**) NC monolayer by NC monolayer degradation mechanism.

As shown in **Figure 4D,** the $t_{1/2}$ for 2L is 40.5 hrs, 3L is 47.1 hrs and for 4L is 61.4 hrs. **Figure 4E** plots the linear increase in $t_{1/2}$ with an increase with the starting E_g absorptance, which we use as a proxy for thickness as it normalizes out any optical density differences. Thus, for every 0.1 (10%) increase in the film E_g absorptance, the $\tau_{1/2}$ is extended by 12.5 hours in the highest quality films. This linear relationship suggests that the degradation occurs layer by layer, initiated by a film surface mediated reaction that is only accessible through voids in the film created once

the layer of NCs above have been fully photo-oxidized (**Figure 4G**). We emphasize that this reaction is initiated at the film surface and not uniformly at the NC surface which are available throughout the entire film depth. To test this notion, a time of flight-secondary ion mass spectrometry (ToF-SIMS) depth profile (**Figure 4F**) was performed on a partially degraded (**Figure S9**) NC film on glass. The Pb signal stays relatively constant across the depth of the film, whereas there is an increase in O and a decrease in I at the surface as compared to the middle or bottom of film. This is in contrast to a fresh NC film, where there is minimal change in the I or O signal throughout the entire depth of the NC film (**Figure S9**). The aged ToF-SIMS depth profile confirms that degradation in a thick NC film occurs NC monolayer by NC monolayer (**Figure 4G**). The observation is fully consistent with our proposed chemical degradation mechanism *via* photo-oxidation that is initiated by surface defects and adsorbed surface species. In the thicker films, buried layers may initially have the benefit of being less accessible to the various adsorbed species contributing to the photo-oxidative degradation process, but will inevitably degrade if catalytic moisture remains present. This also indicates that any imperfections in the NC film, such as variations in the packing density, pinholes or areas of aggregates, all of which can vary dramatically with processing, will impact the photo-oxidation rate as seen by the shorter $t_{1/2}$ at a given E_g absorptance in **Figure 4E**.

Strategies to Mitigate NC Surface Chemistries Associated with Degradation. Based on our proposed mechanism concerning all aspects of the photo-oxidation processes for thick, solar cell relevant $CsPbI_3$ NC films, we identify four rationally designed strategies for mitigating these deleterious reactions. First, simply by increasing the NC film thickness, the lifetime can be extended significantly (**Figure 4D**). Beyond this, the three additional strategies involve judicious control over the surface chemistries that minimize oxidation, which include 1) minimizing the number of under-coordinated surface sites, 2) slowing down the volatilization of surface species or 3) scavenging O_2 from the surface. We emphasize that these methods focus on minimizing the formation of $O_2^{\bullet-}$ which is in contrast to the commonly argued method of improving stability through removing H_2O since we have shown that humidity does not exacerbate $CsPbI_3$ NC degradation.[5] Again, all NC films were aged under illumination and at high humidity (~45% RH).

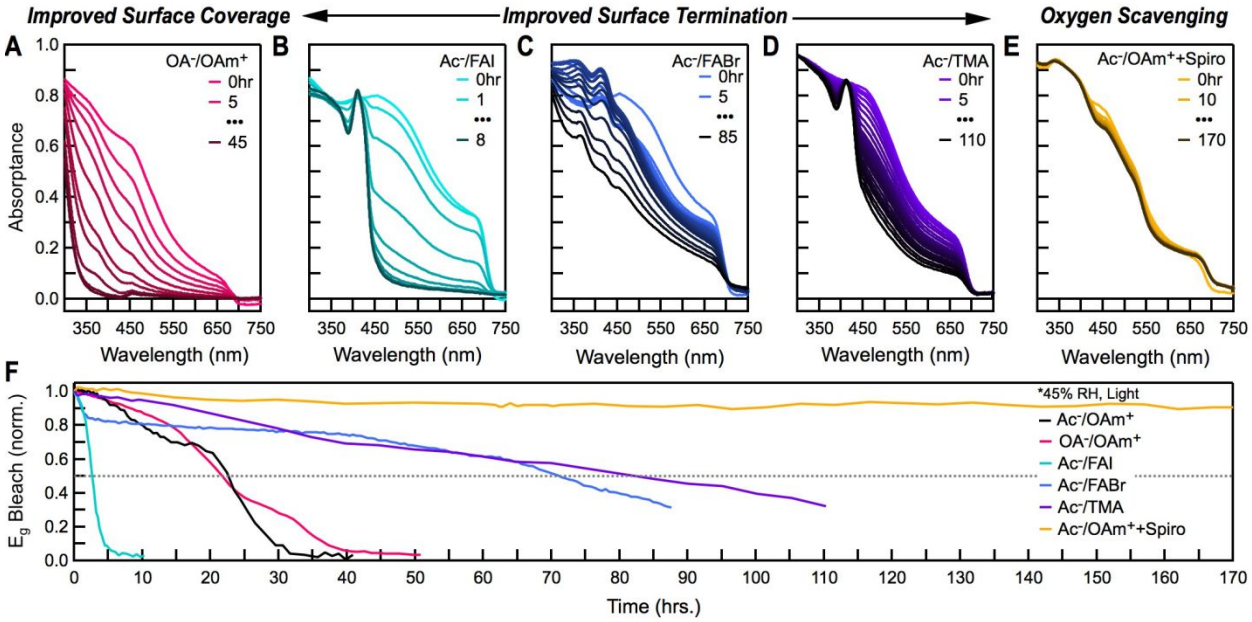

Figure 5: Absorptance spectra over time of NC films testing methods for improve stability by **A**) minimizing undercoordinated surface species with unwashed NCs (OA^-/OAm^+), additional ligand treatments utilizing **B**) formamidinium iodide (FAI), **C**) formamidinium bromide (FABr) salts, **D**) trimethylaluminum (TMA) and **E**) encapsulation with a layer of an O_2 scavenging material spiro-OMeTAD (Spiro). Each absorptance spectrum shown is taken at an equal time interval (hrs) until the last time point as noted in the legend. **F**) Normalized E_g absorption bleach over time for Ac^-/OAm^+ (black), OA^-/OAm^+ (pink), Ac^-/FAI (light blue), Ac^-/FABr (dark blue), Ac^-/TMA (purple) and Ac^-/OAm^++Spiro (yellow) treated NC films under illumination at 45% RH.

To probe the influence of under-coordinated surface sites, we compared photobleaching dynamics of unwashed NCs with the native oleate and oleylammonium (OA^-/OAm^+) ligands intact to washed NCs after ligand exchange. While the ligand exchange of oleate for acetate is critical for improving the charge transport in NC films, the ligand exchange typically leaves under-coordinated surface species, as evidenced by the shorter time-resolved photoluminescence lifetimes (**Figure S10**) as well as smaller relative photoluminescence (PL) intensities (**Figure S11**).[1,9,54] Thus, the OA^-/OAm^+ NCs are a good model system to understand the influence of surface coverage/undercoordinated surface sites on NCs. The $t_{1/2}$ for OA^-/OAm^+ NCs is 20.5 hrs (**Figure 5A**), which is comparable, if not slightly better when thickness is taken into account (**Figure S17**), to that of Ac^-/OAm^+, either meaning that the post-synthesis washing increases the number of under-coordinated sites or that even the existence of a few under-coordinated sites will cause full degradation by a self-propagating photo-oxidation.[46,54] Regardless, a real, but not dramatic difference is observed between the bleaching dynamics of washed *versus* unwashed NCs.

To slow down the volatilization of surface species by improving termination at the NC surface, we tested three different, previously reported, ligand treatments (**Figure S12**) by varying both the ligand salt A and X ions: formamidinium iodide (FAI) (**Figure 5B**), formamidinium bromide (FABr) (**Figure 5C**) and trimethylaluminum (TMA) (**Figure 5D**).[5,9,70] We note that the X site interaction is not a ligand exchange, but an additional surface treatment that occurs from the ligand salt treatment. The FAI salt ligand exchange is commonly used in high efficiency perovskite NC solar cells to improve the NC film conductivity and has led to the champion quantum dot solar cell efficiency of 16.6%.[9,10,12] NC films treated with each of these ligand salts photo-oxidize to a bleached spectrum dominated by a strong peak at ~410 nm, again, likely due to the formation of a 2D species.[69] However, Ac^-/FAI treated NC films have a $t_{1/2}$ of only 2.7 hrs as compared to Ac^-/FABr treated NC films which have a long $t_{1/2}$ of 71.1 hrs. This suggests that the A site in the AX ligand treatment plays a less critical role than the X site in improving the stability, beyond its propensity to be deprotonated by the ROS (**Figure S13**). This is further confirmed by comparing NC films treated with a significantly larger A site ligand salt treatments, phenyltrimethyl ammonium (PTA) iodide and bromide salts, where the former has a $t_{1/2}$ of 1.2 hrs and the latter has a $t_{1/2}$ of 60.4 hrs (**Figures S14, S15**). We note that these ligand salt treatments do not improve the relative PL intensity (**Figure S11**), suggesting that the large changes in $t_{1/2}$ are not primarily driven by the amount of surface passivation. This ligand exchange is different from the ligand surface treatments often used in PC films, where the exchange swaps NC surface ligands and often decreases the PL whereas a PC treatment often improves the PL.[54] Possible reasons bromide surface termination could slow down photo-oxidation include the Pb-Br bond being stronger than the Pb-I bond, increasing the energy necessary to remove Br^-.[71] The success of the ABr surface treatments found here is consistent with a range of literature reports on bromide-containing or bromide-terminated polycrystalline perovskites that demonstrate stability improvements against degradation mediated by moisture, oxygen and light.[27,32,71–78] To further improve NC surface termination, a TMA vapor phase post treatment was tested. TMA is a Lewis acid that often undergoes reacts with surface -OH and -H species in Al_2O_3 atomic layer deposition (ALD) processes, leaving a $-Al(CH_3)_x$ (x=1,2) terminated surface behind, akin to a ligands exchange.[79,80] As a result, the TMA treated film had the longest $t_{1/2}$ of 82.4 hrs. The success of TMA is likely due to the low volatility of Al and ability to passivate under-coordinated surface species, thereby sufficiently stabilizing the NC films. In addition to this benefit, the $-Al(CH_3)_x$ (x=1,2) surface

groups can readily react with H_2O and/or ROS radicals at ambient conditions, leading to aluminum oxide-like species on the NC surface, further aiding the surface stabilization. Excellent solar cell passivation properties have been attributed to nanometer thin Al_2O_3 films, and we expect that similar Al-surface structures also contribute to the stability observed in the TMA-treated samples.[18,81] Clearly, strategies that improve the surface termination of perovskite NCs are quite effective for also enhancing stability.

Arguably, reactive oxygen species play by far the most destructive role in our perovskite NC degradation mechanism, and therefore mitigating their presence should lead to an equally large improvement in stability. Unfortunately, stopping O_2 from forming $O_2^{\bullet-}$ and subsequent ROS through photo-oxidation reactions means removing light from the equation, which is not ideal for a photovoltaic material. Alternatively, O_2 adsorbed to the NC surface could be scavenged before initiating any degradation. To test an oxygen scavenging strategy, we encapsulated an Ac^-/OAm^+ NC film with a known oxygen scavenger (**Figure 5E**): doped (LiTFSI, tBP) spiro-OMeTAD.[82,83] The spiro-OMeTAD encapsulated NC film only degraded to ~90% of the initial absorptance and never reached $t_{1/2}$ during the 170 hr long experiment. It is also possible that spiro-OMeTAD could be scavenging holes, slowing down the degradation reactions. We also encapsulated NC films with polystyrene to deconvolute the effect of encapsulation against both oxygen and water versus oxygen-scavenging effects and found ~80% degradation with polystyrene over the same time period (**Figure S16**), suggesting that the additional scavenging from spiro-OMeTAD is indeed effective.

Conclusion

We report here that $CsPbI_3$ NC films show pronounced stability compared to thin film all-inorganic polycrystalline $CsPbI_3$. Rather than a metastable perovskite phase relaxation, NC films retain the perovskite phase yet follow a slow surface mediated photo-oxidation bleaching that can be mitigated. Reactive oxygen species are responsible for the bleaching of $CsPbI_3$ NC films, which causes the deprotonation of ligands, evolution of iodine and formation of metal carbonate species. Based on all of the ageing experiments (**Table S1, Figure S17**) we postulate that the most stable $CsPbI_3$ NC film for optoelectronic devices would either maintain the native oleylammonium as the amine ligand or utilize terminating ligand salts containing bromide (such as FABr, PTABr) or TMA to reduce volatile, undercoordinated sites that contribute significantly to photo-oxidative

degradation. Since surface chemistries are crucial in degradation rates at both the nanocrystal and bulk levels, the films should be thick, compact, and uniformly continuous. The use of simple encapsulants such as polystyrene will also significantly extend the lifetime. Beyond encapsulation, incorporating an O_2 scavenger, such as Spiro-OMeTAD provides additional protection against photobleaching by reducing chemistry manifolds that lead to highly destructive ROS. By moving beyond controlling surface strain to tailoring the surface chemistry, we have shown multiple methods that stabilize $CsPbI_3$ NCs in ambient atmosphere that should translate to improvements in both PV and LED stability.[84]

Experimental Methods

Materials. All chemicals were used as received from Sigma-Aldrich, unless otherwise specified. Cesium Carbonate (Cs_2CO_3; 99.9%), Oleic Acid (technical grade, 90%), Oleylamine (technical grade, 70%), 1-Octadecene (1-ODE; technical grade, 90%), hexane (reagent grade, ≥95%), Octane (anhydrous, ≥99%), Methyl Acetate (MeOAc, anhydrous, 99.5%), Lead Nitrate ($Pb(NO_3)_2$, 99.999%), Cesium Iodide (CsI, 99.999%), Chlorobenzene (anhydrous, 99.8%), 4-tert-Butylpyridine (tBP; 96%). 2,2′,7,7′- tetrakis(N,N-di-p methoxyphenylamine)-9,9′-spirobifluorene (spiro-OMeTAD; ≥99.5% was purchased from Lumtec. PbI_2 (99.9985%) was purchased from Alfa Aesar.

$CsPbI_3$ NC synthesis. $CsPbI_3$ NCs have been synthesized using high temperature colloidal method and purified as reported by earlier literature.[1,2] Briefly, 500mg PbI_2 was taken in 25 ml 1-ODE and degassed under vacuum at 120 ^oC for 30 minutes. A mixture of 2.5 ml oleylamine and 2.5 ml oleic acid, preheated to 120 ^oC, was injected into the reaction flask. The mixture was briefly degassed until the PbI_2 dissolved to form a light yellowish clear solution. Then the reaction mixture was switched to N_2 and heated up to 180 ^oC. At 180 ^oC, 2 ml of the Cs-oleate solution prepared by mixing 0.407 g of Cs_2CO_3, 20 ml 1-ODE and 1.25 ml oleic acid was swiftly injected into the PbI_2 mixture, and the reaction mixture was immediately quenched in an ice-water bath. The $CsPbI_3$ NCs were isolated by adding 70 ml of MeOAc and centrifuging at 7500 RPM for 5 minutes. The precipitate was then dispersed in 5 ml hexane, reprecipitated with 5 mL MeOAc and centrifuged again at 7500 RPM for 5 minutes. The NCs were finally dispersed in 15 ml hexane and stored at around 2-3 ^oC until used. The final ink for film deposition was prepared by centrifuging the $CsPbI_3$ NCs stock solution at 7500 RPM for 5 minutes, discarding the precipitate, evaporating the hexane from the supernatant and the finally re-dispersing the NCs in 1-2 ml of octane. The NCs ink was filtered through 0.20 μm nylon filter just before spin-casting.

$CsPbI_3$ NC film fabrication. Glass slides were cleaned by sonicating in isopropyl alcohol for 15 minutes followed by UV-ozone for 15 minutes. ~40 ul of a concentrated solution (~60 mg/mL) of $CsPbI_3$ NCs in octane was deposited onto glass, unless otherwise noted, and then spun at 1000 r.p.m for 20 s followed by 2000 r.p.m for 5 s in air at a controlled humidity of 15-22%. Immediately after the sample was done spinning, the substrate was swiftly dipped in a solution of $PbNO_3$ in anhydrous methyl acetate (1 mg/1 mL) and then rinsed in a solution of anhydrous methyl acetate and finally dried with a stream of N_2. This exchanges the oleate (OA^-) ligand for

acetate (Ac^-). For thicker films, this was repeated to build up the desired number of layers (1-4 used here).

Polycrystalline (PC) $CsPbI_3$ thin film deposition. Glass slides cleaned as done for NC film fabrication and then the deposition of the perovskite polycrystalline film was done in a nitrogen glovebox. The precursor solution is a 1M solution with a 1:1.05 CsI:PbI_2 mole ratio in a 4:1 DMF:DMSO solvent mixture. The solution was vortexed until dissolved and filtered using a 200 nm nylon filter before deposition. The films were deposited by spin-coating 45 µl of solution at 1500 r.p.m. for 45 sec and with 10 s of time remaining in the spin procedure 150 µl of methyl acetate was added, as previously reported.[41] The films were annealed at 330 °C for 10 min.

$CsPbI_3$ NC alkylammonium ligand exchange. $CsPbI_3$ NC films were brought into air at controlled humidity 0-5%. Films were dipped into 5 mM solution of AX salt (FAI, FABr, PTAI, PTABr) in methyl acetate for 10 s, followed by a 5 s wash in methyl acetate, to exchange OAm^+ ligands with AX ligands.

Film Encapsulation. A 10mg/mL solution of polystyrene dissolved in toluene was used. The spiro-OMeTAD solution is identical to what is commonly used in devices: 72 mg/ml Spiro-OMeTAD, 28.8 µl/ml tert-butylpyridine (tBP), 17.5 µl LiTFSI stock solution (520mg/ml in acetonitrile) dissolved in chlorobenzene. Solutions were spun in air at low humidity (<10 %) at 5000 rpm for 30 s.

$CsPbI_3$ NC trimethylaluminium (TMA) surface treatment. The $CsPbI_3$ Ac^-/OAm^+ NCs were inserted in Beneq TFS 200 ALD reactor at a temperature T~45˚C and were pumped on to reach a base pressure of ~1 mTorr. Subsequently, the NC samples were subjected to 15 pulses of trimethylaluminum (TMA) of 2 s each and separated by 1-min N_2 purging steps.

Time-dependent absorptance. The same custom-built instrument used in this work is described in detail in our previous work.[85] It essentially consists of a halogen lamp array (Sylvania 58321) outputting 120 mW/cm^2 and two spectrometers (Ocean Optics HR2000) fitted with a 'six around one' reflectance probe (Ocean Optics R400-7-SR) and a collimating lens to capture reflectance and transmission measurements respectively which were used to calculate true absorptance.

x-ray diffraction (XRD). Measurements were collected in air on a zero-background single-crystalline Si XRD plate using a Bruker D8 Discover diffractometer with a GADDS 4-circle detector (General Area Detector Diffraction System) and a Cu Kα (1.5406 Å, 8.04 eV) X-ray source. ISCD reference patterns were used to compare against experimentally measured XRD patterns, specifically $PbCO_3 \bullet H_2O$ (280932), $PbCO_3$ (6178) and Cs_2CO_3 (14156)

x-ray photoelectron spectroscopy (XPS). XPS measurements were performed in a Kratos AXIS Nova system (base pressures below 2×10^{-9} Torr) using monochromatic Al Kα X-ray excitation ($h\nu$ = 1486.7 eV). Measurements were performed with 40 eV pass energy, and spectrometer binding-energy scale was calibrated by measuring valence-band and core-level spectra from sputter-cleaned Au, Ag, and Cu foils (E_F = 0.00 eV, Au $4f_{7/2}$ = 83.96 eV, Ag $3d_{5/2}$ = 368.26 eV, and Cu $2p_{3/2}$ = 932.62 eV).[86]

Fourier transform infrared spectroscopy (FTIR). FTIR measurements were done using a Bruker Alpha FTIR spectrometer using a diffuse reflectance infrared Fourier transform spectrometer (DRIFTS) attachment with a resolution of 4 cm^{-1} on gold-coated, polished Si wafer substrates. Background measurements were taken on blank substrates and subsequent sample measurements were taken as an average of 24 scans. Spectra were baseline-corrected using the concave rubberband correction method. To obtain FTIR of a partially degraded NC film, a fresh NC film was drop-cast on the substrate and first a FTIR spectra was taken of the fresh sample. The sample was then allowed to degrade under ambient conditions (low humidity and in the dark) without being removed from the FTIR until it had partially degraded and then a FTIR spectra was taken. For the fully degraded FTIR, NCs were spincoated on the substrates and fully degraded (humid, light) before FTIR was taken in an Ar glovebox.

Time of flight – secondary ion mass spectrometry (ToF-SIMS). An ION-TOF TOF-SIMS V Time of Flight SIMS (TOF-SIMS) spectrometer was utilized for depth profiling and chemical imaging of the perovskite utilizing methods covered in detail in previous reports.[87–89] Analysis was completed utilizing a 3-lens 30kV BiMn primary ion gun. Depth profiles were completed with the Bi_3^+ primary ion beam, (0.8pA pulsed beam current), a 50x50µm area was analyzed with a 128:128 primary beam raster (below a primary ion dose density of 1×10^{12} ions cm^{-2} to remain at the static-sims limit). Sputter depth profiling was accomplished with 1KeV Cesium and 1KeV oxygen ion sputter beams (4.6 and 3.5 nA sputter current, respectively) with a raster of 150×150 microns. After completion of the SIMS measurements the depth of the craters was determined by optical interference light microscopy, to convert the SIMS sputter time scale to a sputter depth scale.

Time resolved photoluminescence spectroscopy (TRPL). Time-resolved photoluminescence (TRPL) films was measured using a supercontinuum fiber laser (NKT Photonics, Super K) operating at 5 MHz as the excitation source. Films were excited at 500 nm at a low fluence ($<< 10^{15}$ s^{-1}) and a Hamamatsu C10910−04 streak camera was used to collect time-resolved spectra. Bi-exponential fits of the TRPL decays were weighted to calculate the average PL lifetime using the equation: $\tau_{avg} = (A_0\tau_0 + A_1\tau_1)/(A_0 + A_1)$.

Supplemental Information:

The supplemental information includes additional characterization of fully aged $CsPbI_3$ polycrystalline, partially and fully aged nanocrystal films (XRD, XPS, FTIR, SEM, ToF-SIMS). Additional characterization of ligand treated NC films (TRPL, PL, FTIR). Stability of $CsPbI_3$ NC films aged in the dark, in water, with PTAI and PTABr salt ligand treatments as well as encapsulated with polystyrene. Finally, a summary of all stability data reported herein is compiled.

Acknowledgements:

This work was authored in part by the Alliance for Sustainable Energy, Limited Liability Company, the manager and operator of the National Renewable Energy Laboratory under Contract No. DE-AC36-08GO28308. The views expressed in the article do not necessarily represent the views of the Department of Energy or the U.S. Government. T.M., A.H., J.R.P. and J.M.L. acknowledge the Operational Energy Capability Improvement Fund of the Department of Defense. D.R.D. acknowledges the U.S. DOE, office of Science, Office of Workforce

Development for Teachers and Scientists, Science Undergraduate Laboratory Internship (SULI) Program for funding in 2018 and 2019. T.H.S. acknowledges the Department of Chemistry at the Colorado School of Mines for financial support through teaching assistantships and a Graduate Research Fellowship award. S.N.H. acknowledges support from the NREL directors fellowship LDRD program. Funding for B.R and L.M.W. provided by the Building Technologies Offices within the U.S. Department of Energy Office of Energy Efficiency and Renewable Energy.

References:

(1) Swarnkar, A.; Marshall, A. R.; Sanehira, E. M.; Chernomordik, B. D.; Moore, D. T.; Christians, J. A.; Chakrabarti, T.; Luther, J. M. Quantum Dot-Induced Phase Stabilization of Alpha-CsPbI3 Perovskite for High Efficiency Photovoltaics. *Science* **2016**, *354* (6308), 92–95. https://doi.org/10.1126/science.aag2700.

(2) Hazarika, A.; Zhao, Q.; Gaulding, E. A.; Christians, J. A.; Dou, B.; Marshall, A. R.; Moot, T.; Berry, J. J.; Johnson, J. C.; Luther, J. M. Perovskite Quantum Dot Photovoltaic Materials beyond the Reach of Thin Films: Full-Range Tuning of A-Site Cation Composition. *ACS Nano* **2018**, *12* (10), 10327–10337. https://doi.org/10.1021/acsnano.8b05555.

(3) Song, J.; Li, J.; Xu, L.; Li, J.; Zhang, F.; Han, B.; Shan, Q.; Zeng, H. Room-Temperature Triple-Ligand Surface Engineering Synergistically Boosts Ink Stability , Recombination Dynamics , and Charge Injection toward EQE-11 . 6 % Perovskite QLEDs. *Advanced Materials* **2018**, *30*, 1800764. https://doi.org/10.1002/adma.201800764.

(4) Capello, C.; Fischer, U.; Hungerbühler, K. What Is a Green Solvent? A Comprehensive Framework for the Environmental Assessment of Solvents. *Green Chemistry* **2007**, *9* (9), 927–934. https://doi.org/10.1039/b617536h.

(5) Yuan, J.; Bi, C.; Wang, S.; Guo, R.; Shen, T.; Zhang, L. Spray-Coated Colloidal Perovskite Quantum Dot Films for Highly Efficient Solar Cells. *Advanced Functional Materials* **2019**, *29*, 1906615. https://doi.org/10.1002/adfm.201906615.

(6) Yuan, J.; Ling, X.; Yang, D.; Li, F.; Zhou, S.; Shi, J.; Qian, Y.; Hu, J.; Sun, Y.; Yang, Y.; et al. Band-Aligned Polymeric Hole Transport Materials for Extremely Low Energy Loss α-CsPbI3 Perovskite Nanocrystal Solar Cells. *Joule* **2018**, *2* (11), 2450–2463. https://doi.org/10.1016/j.joule.2018.08.011.

(7) Dai, S. W.; Hsu, B. W.; Chen, C. Y.; Lee, C. A.; Liu, H. Y.; Wang, H. F.; Huang, Y. C.; Wu, T. L.; Manikandan, A.; Ho, R. M.; et al. Perovskite Quantum Dots with Near Unity Solution and Neat-Film Photoluminescent Quantum Yield by Novel Spray Synthesis. *Advanced Materials* **2018**, *30* (7), 1705532. https://doi.org/10.1002/adma.201705532.

(8) Pan, J.; Shang, Y.; Yin, J.; De Bastiani, M.; Peng, W.; Dursun, I.; Sinatra, L.; El-Zohry, A. M.; Hedhili, M. N.; Emwas, A. H.; et al. Bidentate Ligand-Passivated CsPbI 3 Perovskite Nanocrystals for Stable Near-Unity Photoluminescence Quantum Yield and Efficient Red Light-Emitting Diodes. *Journal of the American Chemical Society* **2018**, *140* (2), 562–565. https://doi.org/10.1021/jacs.7b10647.

(9) Sanehira, E. M.; Marshall, A. R.; Christians, J. A.; Harvey, S. P.; Ciesielski, P. N.; Wheeler, L. M.; Schulz, P.; Lin, L. Y.; Beard, M. C.; Luther, J. M. Enhanced Mobility CsPbI3 Quantum Dot Arrays for Record-Efficiency, High-Voltage Photovoltaic Cells. *Science Advances* **2017**, *3* (10), aao4204. https://doi.org/10.1126/sciadv.aao4204.

(10) Zhao, Q.; Hazarika, A.; Chen, X.; Harvey, S. P.; Larson, B. W.; Teeter, G. R.; Liu, J.;

Song, T.; Xiao, C.; Shaw, L.; et al. High Efficiency Perovskite Quantum Dot Solar Cells with Charge Separating Heterostructure. *Nature Communications* **2019**, *10* (2842), 2842. https://doi.org/10.1038/s41467-019-10856-z.

(11) Li, F.; Zhou, S.; Yuan, J.; Qin, C.; Yang, Y.; Shi, J.; Ling, X.; Li, Y. Perovskite Quantum Dot Solar Cells with 15.6% Efficiency and Improved Stability Enabled by an Alpha-CsPbI3/FAPbI3 Bilayer Structure. *ACS Energy Letters* **2019**, *4*, 2571–2578. https://doi.org/10.1021/acsenergylett.9b01920.

(12) Hao, M.; Bai, Y.; Zeiske, S.; Ren, L.; Liu, J.; Yuan, Y.; Zarrabi, N.; Cheng, N.; Ghasemi, M.; Chen, P.; et al. Ligand-Assisted Cation-Exchange Engineering for High-Efficiency Colloidal Cs1−xFAxPbI3 Quantum Dot Solar Cells with Reduced Phase Segregation. *Nature Energy* **2020**, *5* (1), 79–88. https://doi.org/10.1038/s41560-019-0535-7.

(13) NREL. Best Research-Cell Efficiency Chart https://www.nrel.gov/pv/assets/pdfs/best-research-cell-efficiencies.20190923.pdf (accessed Oct 16, 2019).

(14) Meyns, M.; Pera, M.; Heuer-jungemann, A.; Hertog, W.; Iba, M.; Nafria, R.; Genc, A.; Arbiol, J.; Kovalenko, M. V; Carreras, J.; et al. Polymer-Enhanced Stability of Inorganic Perovskite Nanocrystals and Their Application in Color Conversion LEDs. *ACS Applied Materials & Interfaces* **2016**, *8*, 19579–19586. https://doi.org/10.1021/acsami.6b02529.

(15) Krieg, F.; Ong, Q. K.; Burian, M.; Rainò, G.; Naumenko, D.; Amenitsch, H.; Süess, A.; Grotevent, M. J.; Krumeich, F.; Bodnarchuk, M. I.; et al. Stable Ultraconcentrated and Ultradilute Colloids of CsPbX3 (X = Cl, Br) Nanocrystals Using Natural Lecithin as a Capping Ligand. *Journal of the American Chemical Society* **2020**, *141* (50), 19839–19849. https://doi.org/10.1021/jacs.9b09969.

(16) Krieg, F.; Ochsenbein, S. T.; Yakunin, S.; Ten Brinck, S.; Aellen, P.; Süess, A.; Clerc, B.; Guggisberg, D.; Nazarenko, O.; Shynkarenko, Y.; et al. Colloidal CsPbX3 (X = Cl, Br, I) Nanocrystals 2.0: Zwitterionic Capping Ligands for Improved Durability and Stability. *ACS Energy Letters* **2018**, *3* (3), 641–646. https://doi.org/10.1021/acsenergylett.8b00035.

(17) Huang, H.; Bodnarchuk, M. I.; Kershaw, S. V.; Kovalenko, M. V; Rogach, A. L. Lead Halide Perovskite Nanocrystals in the Research Spotlight: Stability and Defect Tolerance. *ACS Energy Letters* **2017**, *2* (9), 2071–2083. https://doi.org/10.1021/acsenergylett.7b00547.

(18) Loiudice, A.; Saris, S.; Oveisi, E.; Alexander, D. T. L.; Buonsanti, R. Quantum Dots CsPbBr 3 QD / AlO x Inorganic Nanocomposites with Exceptional Stability in Water, Light, and Heat. *Angewandte Chemie* **2017**, *56*, 10696–10701. https://doi.org/10.1002/anie.201703703.

(19) Xuan, T.; Huang, J.; Liu, H.; Lou, S.; Cao, L.; Gan, W.; Liu, R. S.; Wang, J. Super-Hydrophobic Cesium Lead Halide Perovskite Quantum Dot-Polymer Composites with High Stability and Luminescent Efficiency for Wide Color Gamut White Light-Emitting Diodes. *Chemistry of Materials* **2019**, *31* (3), 1042–1047. https://doi.org/10.1021/acs.chemmater.8b04596.

(20) Ma, J.; Yin, J.; Chen, Y.; Zhao, Q.; Zhou, Y.; Li, H.; Kuroiwa, Y.; Miroyoshi, C.; Li, Z.-Y.; Bakr, O. M.; et al. Defect-Triggered Phase Transition in Cesium Lead Halide Perovskite Nanocrystals. *ACS Materials Letters* **2019**, *1*, 185–191. https://doi.org/10.1021/acsmaterialslett.9b00128.

(21) Zhao, Q.; Hazarika, A.; Schelhas, L. T.; Liu, J.; Gaulding, E. A.; Li, G.; Zhang, M.; Toney, M. F.; Sercel, P. C.; Luther, J. M. Size-Dependent Lattice Structure and Confinement Properties in CsPbI3 Perovskite Nanocrystals: Negative Surface Energy for

Stabilization. *ACS Energy Letters* **2020**, *5*, 238–247. https://doi.org/10.1021/acsenergylett.9b02395.

(22) Shi, J.; Li, F.; Yuan, J.; Ling, X.; Zhou, S.; Qian, Y.; Ma, W. Efficient and Stable CsPbI 3 Perovskite Quantum Dots Enabled by in Situ Ytterbium Doping for Photovoltaic Applications . *Journal of Materials Chemistry A* **2019**, *7* (36), 20936–20944. https://doi.org/10.1039/c9ta07143a.

(23) Christians, J. A.; Schulz, P.; Tinkham, J. S.; Schloemer, T. H.; Harvey, S. P.; Tremolet De Villers, B. J.; Sellinger, A.; Berry, J. J.; Luther, J. M. Tailored Interfaces of Unencapsulated Perovskite Solar Cells for >1,000 Hour Operational Stability. *Nature Energy* **2018**, *3* (1), 68–74. https://doi.org/10.1038/s41560-017-0067-y.

(24) Bryant, D.; Aristidou, N.; Pont, S.; Sanchez-Molina, I.; Chotchunangatchaval, T.; Wheeler, S.; Durrant, J. R.; Haque, S. A. Light and Oxygen Induced Degradation Limits the Operational Stability of Methylammonium Lead Triiodide Perovskite Solar Cells. *Energy & Environmental Science* **2016**, *9*, 1655–1660. https://doi.org/10.1039/c6ee00409a.

(25) Leijtens, T.; Eperon, G. E.; Pathak, S.; Abate, A.; Lee, M. M.; Snaith, H. J. Overcoming Ultraviolet Light Instability of Sensitized TiO2 with Meso-Superstructured Organometal Tri-Halide Perovskite Solar Cells. *Nature Communications* **2013**, *4*, 2885. https://doi.org/10.1038/ncomms3885.

(26) Aristidou, N.; Eames, C.; Sanchez-Molina, I.; Bu, X.; Kosco, J.; Saiful Islam, M.; Haque, S. A. Fast Oxygen Diffusion and Iodide Defects Mediate Oxygen-Induced Degradation of Perovskite Solar Cells. *Nature Communications* **2017**, *8*, 15218. https://doi.org/10.1038/ncomms15218.

(27) Senocrate, A.; Acarturk, T.; Kim, G. Y.; Merkle, R.; Starke, U.; Gratzel, M.; Maier, J. Interaction of Oxygen with Halide Perovskites. *Journal of Materials Chemistry A* **2018**, *6*, 10847–10855. https://doi.org/10.1039/c8ta04537b.

(28) O'Mahony, F. T. F.; Lee, Y. H.; Jellett, C.; Dmitrov, S.; Bryant, D. T. J.; Durrant, J. R.; O'Regan, B. C.; Graetzel, M.; Nazeeruddin, M. K.; Haque, S. A. Improved Environmental Stability of Organic Lead Trihalide Perovskite-Based Photoactive-Layers in the Presence of Mesoporous TiO2. *Journal of Materials Chemistry A* **2015**, *3* (14), 7219–7223. https://doi.org/10.1039/c5ta01221j.

(29) Christians, J. A.; Herrera, P. A. M.; Kamat, P. V. Transformation of the Excited State and Photovoltaic Efficiency of CH3NH3PbI3 Perovskite upon Controlled Exposure to Humidified Air. *Journal of the American Chemical Society* **2015**, *137*, 1530–1538. https://doi.org/10.1021/ja511132a.

(30) Leguy, A. M. A.; Hu, Y.; Campoy-Quiles, M.; Alonso, M. I.; Weber, O. J.; Azarhoosh, P.; Van Schilfgaarde, M.; Weller, M. T.; Bein, T.; Nelson, J.; et al. Reversible Hydration of CH3NH3PbI3 in Films, Single Crystals, and Solar Cells. *Chemistry of Materials* **2015**, *27* (9), 3397–3407. https://doi.org/10.1021/acs.chemmater.5b00660.

(31) Yang, J.; Siempelkamp, B. D.; Liu, D.; Kelly, T. L. Investigation of CH3NH3PbI3degradation Rates and Mechanisms in Controlled Humidity Environments Using in Situ Techniques. *ACS Nano* **2015**, *9* (2), 1955–1963. https://doi.org/10.1021/nn506864k.

(32) Noh, J. H.; Im, S. H.; Heo, J. H.; Mandal, T. N.; Seok, S. Il. Chemical Management for Colorful, Efficient, and Stable Inorganic-Organic Hybrid Nanostructured Solar Cells. *Nano Letters* **2013**, *13* (4), 1764–1769. https://doi.org/10.1021/nl400349b.

(33) Mosconi, E.; Azpiroz, J. M.; De Angelis, F. Ab Initio Molecular Dynamics Simulations of Methylammonium Lead Iodide Perovskite Degradation by Water. *Chemistry of Materials* **2015**, *27*, 4885–4892. https://doi.org/10.1021/acs.chemmater.5b01991.

(34) Huang, W.; Manser, J. S.; Kamat, P. V; Ptasinska, S. Evolution of Chemical Composition, Morphology, and Photovoltaic Efficiency of CH3NH3PbI3 Perovskite under Ambient Conditions. *Chemistry of Materials* **2016**, *28*, 303–311. https://doi.org/10.1021/acs.chemmater.5b04122.

(35) Aristidou, N.; Sanchez-Molina, I.; Chotchuangchutchaval, T.; Brown, M.; Martinez, L.; Rath, T.; Haque, S. A. The Role of Oxygen in the Degradation of Methylammonium Lead Trihalide Perovskite Photoactive Layers. *Angewandte Chemie* **2015**, *54* (28), 8208–8212. https://doi.org/10.1002/anie.201503153.

(36) Christians, J. A.; Habisreutinger, S. N.; Berry, J. J.; Luther, J. M. Stability in Perovskite Photovoltaics: A Paradigm for Newfangled Technologies. *ACS Energy Letters* **2018**, *3* (9), 2136–2143. https://doi.org/10.1021/acsenergylett.8b00914.

(37) Leijtens, T.; Giovenzana, T.; Habisreutinger, S. N.; Tinkham, J. S.; Noel, N. K.; Kamino, B. A.; Sadoughi, G.; Sellinger, A.; Snaith, H. J. Hydrophobic Organic Hole Transporters for Improved Moisture Resistance in Metal Halide Perovskite Solar Cells. *ACS Applied Materials & Interfaces* **2016**, *8* (9), 5981–5989. https://doi.org/10.1021/acsami.5b10093.

(38) Christians, J. A.; Schulz, P.; Tinkham, J. S.; Schloemer, T. H.; Harvey, S. P.; Tremolet de Villers, B. J.; Sellinger, A.; Berry, J. J.; Luther, J. M. Tailored Interfaces of Unencapsulated Perovskite Solar Cells for >1,000 Hour Operational Stability-SI. *Nature Energy* **2018**, *3* (1), 68–74. https://doi.org/10.1038/s41560-017-0067-y.

(39) Liu, Y.; Akin, S.; Pan, L.; Uchida, R.; Arora, N.; Milić, J. V; Hinderhofer, A.; Schreiber, F.; Uhl, A. R.; Zakeeruddin, S. M.; et al. Ultrahydrophobic 3D/2D Fluoroarene Bilayer-Based Water-Resistant Perovskite Solar Cells with Efficiencies Exceeding 22 %. *Science Advances* **2019**, *5*, eaaw2543. https://doi.org/10.1126/sciadv.aaw2543.

(40) Wheeler, L. M.; Sanehira, E. M.; Marshall, A. R.; Schulz, P.; Suri, M.; Anderson, N. C.; Christians, J. A.; Nordlund, D.; Sokaras, D.; Kroll, T.; et al. Targeted Ligand-Exchange Chemistry on Cesium Lead Halide Perovskite Quantum Dots for High-Efficiency Photovoltaics. *Journal of the American Chemical Society* **2018**, *140* (33), 10504–10513. https://doi.org/10.1021/jacs.8b04984.

(41) Moot, T.; Marshall, A. R.; Wheeler, L. M.; Habisreutinger, S. N.; Schloemer, T. H.; Boyd, C. C.; Dikova, D. R.; Pach, G. F.; Hazarika, A.; McGehee, M. D.; et al. CsI-Antisolvent Adduct Formation in All-Inorganic Metal Halide Perovskites. *Advanced Energy Materials* **2020**, *10* (9), 1903365. https://doi.org/10.1002/aenm.201903365.

(42) Straus, D. B.; Guo, S.; Cava, R. J. Kinetically Stable Single Crystals of Perovskite-Phase CsPbI3. *Journal of the American Chemical Society* **2019**, *141* (29), 11435–11439. https://doi.org/10.1021/jacs.9b06055.

(43) Shirayama, M.; Kato, M.; Miyadera, T.; Sugita, T.; Fujiseki, T.; Hara, S.; Kadowaki, H.; Murata, D.; Chikamatsu, M.; Fujiwara, H. Degradation Mechanism of CH3NH3PbI3 Perovskite Materials upon Exposure to Humid Air. *Journal of Applied Physics* **2016**, *119* (11). https://doi.org/10.1063/1.4943638.

(44) Akkerman, Q. A.; Park, S.; Radicchi, E.; Nunzi, F.; Mosconi, E.; De Angelis, F.; Brescia, R.; Rastogi, P.; Prato, M.; Manna, L. Nearly Monodisperse Insulator Cs4PbX6 (X= Cl, Br, I) Nanocrystals, Their Mixed Halide Compositions, and Their Transformation into CsPbX 3 Nanocrystals. *Nano Letters* **2017**, *17*, 1934–1930.

https://doi.org/10.1021/acs.nanolett.6b05262.

(45) Andrews, L.; Hwang, J.; Trindle, C. Matrix Reactions of Cesium Atoms with Oxygen Molecules. Infrared Spectrum and Vibrational Analysis of Cs + 02- . Infrared Observation of Cs + 022-Cs +. *Journal of Physical Chemistry* **1973**, *77* (8), 1065–1068. https://doi.org/10.1021/j100627a020.

(46) Fu, F.; Pisoni, S.; Jeangros, Q.; Sastre-Pellicer, J.; Kawecki, M.; Paracchino, A.; Moser, T.; Werner, J.; Andres, C.; Duchêne, L.; et al. I2 Vapor-Induced Degradation of Formamidinium Lead Iodide Based Perovskite Solar Cells under Heat–Light Soaking Conditions. *Energy & Environmental Science* **2019**, *12*, 3074–3088. https://doi.org/10.1039/c9ee02043h.

(47) Jain, A.; Ong, S. P.; Hautier, G.; Chen, W.; Richards, W. D.; Dacek, S.; Cholia, S.; Gunter, D.; Skinner, D.; Ceder, G.; et al. Commentary: The Materials Project: A Materials Genome Approach to Accelerating Materials Innovation. *APL Materials* **2013**, *1* (1), 011002. https://doi.org/10.1063/1.4812323.

(48) He, J.; Fang, W. H.; Long, R.; Prezhdo, O. V. Superoxide/Peroxide Chemistry Extends Charge Carriers' Lifetime but Undermines Chemical Stability of CH3NH3PbI3 Exposed to Oxygen: Time-Domain Ab Initio Analysis. *Journal of the American Chemical Society* **2019**, *141* (14), 5798–5807. https://doi.org/10.1021/jacs.8b13392.

(49) Zhang, L.; H.L. Sit, P. Ab Initio Study of the Role of Oxygen and Excess Electrons in the Degradation of CH3NH3PbI3. *Journal of Materials Chemistry A* **2017**, *5*, 9042–9049. https://doi.org/10.1039/c7ta01091e.

(50) Motti, S. G.; Meggiolaro, D.; Barker, A. J.; Mosconi, E.; Andrea, C.; Perini, R.; Ball, J. M.; Gandini, M.; Kim, M.; Angelis, F. De; et al. Controlling Competing Photochemical Reactions Stabilizes Perovskite Solar Cells. *Nature Photonics* **2019**, *13*, 532–539. https://doi.org/10.1038/s41566-019-0435-1.

(51) Evarestov, R. A.; Senocrate, A.; Kotomin, E. A.; Maier, J. First Principles Calculations of Iodine-Related Point Defects in CsPbI3. *Phys. Chem. Chem. Phys.* **2019**, *21*, 7841–7846. https://doi.org/10.1039/c9cp00414a.

(52) Ouyang, Y.; Li, Y.; Zhu, P.; Li, Q.; Gao, Y.; Tong, J.; Shi, L.; Zhou, Q.; Ling, C.; Chen, Q.; et al. Photo-Oxidative Degradation of Methylammonium Lead Iodide Perovskite: Mechanism and Protection. *Journal of Materials Chemistry A* **2019**, *7* (5), 2275–2282. https://doi.org/10.1039/c8ta12193a.

(53) Péan, E. V.; De Castro, C. S.; Dimitrov, S.; De Rossi, F.; Meroni, S.; Baker, J.; Watson, T.; Davies, M. L. Investigating the Superoxide Formation and Stability in Mesoporous Carbon Perovskite Solar Cells with an Aminovaleric Acid Additive. *Advanced Functional Materials* **2020**, *30* (12), 1909839. https://doi.org/10.1002/adfm.201909839.

(54) Li, J.; Xu, L.; Wang, T.; Song, J.; Chen, J.; Xue, J.; Dong, Y.; Cai, B.; Shan, Q.; Zeng, H. 50-Fold EQE Improvement up to 6.27 % of Solution-Processed All-Inorganic Perovskite CsPbBr 3 QLEDs via Surface Ligand Density Control. *Advanced Materials* **2017**, *29*, 1603885. https://doi.org/10.1002/adma.201603885.

(55) Grisorio, R.; Di Clemente, M. E.; Fanizza, E.; Allegretta, I.; Altamura, D.; Striccoli, M.; Terzano, R.; Giannini, C.; Irimia-Vladu, M.; Suranna, G. P. Exploring the Surface Chemistry of Cesium Lead Halide Perovskite Nanocrystals. *Nanoscale* **2019**, *11*, 986–999. https://doi.org/10.1039/c8nr08011a.

(56) De Roo, J.; Ibáñez, M.; Geiregat, P.; Nedelcu, G.; Walravens, W.; Maes, J.; Martins, J. C.; Van Driessche, I.; Kovalenko, M. V; Hens, Z. Highly Dynamic Ligand Binding and Light

Absorption Coefficient of Cesium Lead Bromide Perovskite Nanocrystals. *ACS Nano* **2016**, *10* (2), 2071–2081. https://doi.org/10.1021/acsnano.5b06295.

(57) Gonzalez, V.; Wallez, G.; Calligaro, T.; Gourier, D.; Menu, M. Synthesizing Lead White Pigments by Lead Corrosion: New Insights into the Ancient Manufacturing Processes. *Corrosion Science* **2019**, *146* (July 2018), 10–17. https://doi.org/10.1016/j.corsci.2018.10.033.

(58) Leijtens, T.; Prasanna, R.; Gold-Parker, A.; Toney, M. F.; McGehee, M. D. Mechanism of Tin Oxidation and Stabilization by Lead Substitution in Tin Halide Perovskites. *ACS Energy Letters* **2017**, *2* (9), 2159–2165. https://doi.org/10.1021/acsenergylett.7b00636.

(59) Xie, G.; Xu, L.; Sun, L.; Xiong, Y.; Wu, P.; Hu, B. Insight into the Reaction Mechanism of Water, Oxygen and Nitrogen Molecules on a Tin Iodine Perovskite Surface. *Journal of Materials Chemistry A* **2019**, *7* (10), 5779–5793. https://doi.org/10.1039/c8ta11705e.

(60) Hayyan, M.; Hashim, M. A.; AlNashef, I. M. Superoxide Ion : Generation and Chemical Implications. *Chemical Reviews* **2016**, *116*, 3029–3085. https://doi.org/10.1021/acs.chemrev.5b00407.

(61) Bray, W. C.; Liebhafsky, H. A. Reactions Involving Hydrogen Peroxide, Iodine and Iodate Ion. I. Introduction. *Journal of the American Chemical Society* **1931**, *53* (1), 38–44. https://doi.org/10.1021/ja01352a006.

(62) Brenes, R.; Eames, C.; Bulović, V.; Islam, M. S.; Stranks, S. D. The Impact of Atmosphere on the Local Luminescence Properties of Metal Halide Perovskite Grains. *Advanced Materials* **2018**, *30* (15), 1706208. https://doi.org/10.1002/adma.201706208.

(63) Godding, J. S. W.; Ramadan, A. J.; Lin, Y. H.; Schutt, K.; Snaith, H. J.; Wenger, B. Oxidative Passivation of Metal Halide Perovskites. *Joule* **2019**, *3* (11), 2716–2731. https://doi.org/10.1016/j.joule.2019.08.006.

(64) Yang, S.; Chen, S.; Mosconi, E.; Fang, Y.; Xiao, X.; Wang, C.; Zhou, Y.; Yu, Z.; Zhao, J.; Gao, Y.; et al. Stabilizing Halide Perovskite Surfaces for Solar Cell Operation with Wide-Bandgap Lead Oxysalts. *Science* **2019**, *365* (6452), 473–478. https://doi.org/10.1126/science.aax3294.

(65) Davidson, R. S. Chapter 5: The Roles of Amines in UV Curing. In *Radiation curing in polymer science and technology*; 1993; pp 153–176.

(66) Fouassier, J. P.; Rabek, J. F. *Radiation Curing in Polymer Science and Technology. Vol. 1: Fundamentals and Methods*; Elsevier Applied Science: London, 1993.

(67) Ouyang, Y.; Li, Y.; Zhu, P.; Li, Q.; Gao, Y.; Tong, J.; Shi, L.; Zhou, Q.; Ling, C.; Chen, Q.; et al. Photo-Oxidative Degradation of Methylammonium Lead Iodide Perovskite: Mechanism and Protection. *Journal of Materials Chemistry A* **2019**, *7*, 2275–2282. https://doi.org/10.1039/c8ta12193a.

(68) Brennan, M. C.; Toso, S.; Pavlovetc, I. M.; Zhukovskyi, M.; Marras, S.; Kuno, M.; Manna, L.; Baranov, D. Superlattices Are Greener on the Other Side: How Light Transforms Self-Assembled Mixed Halide Perovskite Nanocrystals. *ACS Energy Letters* **2020**, *5* (5), 1465–1473. https://doi.org/10.1021/acsenergylett.0c00630.

(69) Wheeler, L. M.; Anderson, N. C.; Bliss, T. S.; Hautzinger, M. P.; Neale, N. R. Dynamic Evolution of 2D Layers within Perovskite Nanocrystals via Salt Pair Extraction and Reinsertion. *Journal of Physical Chemistry C* **2018**, *122* (25), 14029–14038. https://doi.org/10.1021/acs.jpcc.8b01164.

(70) Saris, S.; Dona, S. T.; Niemann, V.; Loiudice, A.; Buonsanti, R. Optimizing the Atomic Layer Deposition of Alumina on Perovskite Nanocrystal Films by Using O 2 As a

Molecular Probe. *Helvetica Chimica Acta* **2020**, *103*, e2000055. https://doi.org/10.1002/hlca.202000055.

(71) Aziz, A.; Aristidou, N.; Bu, X.; Westbrook, R. J. E.; Haque, S. A.; Islam, M. S. Understanding the Enhanced Stability of Bromide Substitution in Lead Iodide Perovskites. *Chemistry of Materials* **2020**, *32* (1), 400–409. https://doi.org/10.1021/acs.chemmater.9b04000.

(72) Pont, S.; Bryant, D.; Lin, C. T.; Aristidou, N.; Wheeler, S.; Ma, X.; Godin, R.; Haque, S. A.; Durrant, J. R. Tuning CH3NH3Pb(I1-:XBrx)3 Perovskite Oxygen Stability in Thin Films and Solar Cells. *Journal of Materials Chemistry A* **2017**, *5* (20), 9553–9560. https://doi.org/10.1039/c7ta00058h.

(73) Ouafi, M.; Jaber, B.; Atourki, L.; Bekkari, R.; Laânab, L. Improving UV Stability of MAPbI3 Perovskite Thin Films by Bromide Incorporation. *Journal of Alloys and Compounds* **2018**, *746*, 391–398. https://doi.org/10.1016/j.jallcom.2018.02.240.

(74) Ansari, F.; Salavati-Niasari, M.; Nazari, P.; Mir, N.; Ahmadi, V.; Abdollahi Nejand, B. Long-Term Durability of Bromide-Incorporated Perovskite Solar Cells via a Modified Vapor-Assisted Solution Process. *ACS Applied Energy Materials* **2018**, *1* (11), 6018–6026. https://doi.org/10.1021/acsaem.8b01075.

(75) Svanström, S.; Jacobsson, T. J.; Sloboda, T.; Giangrisostomi, E.; Ovsyannikov, R.; Rensmo, H.; Cappel, U. B. Effect of Halide Ratio and Cs+ Addition on the Photochemical Stability of Lead Halide Perovskites. *Journal of Materials Chemistry A* **2018**, *6* (44), 22134–22144. https://doi.org/10.1039/c8ta05795h.

(76) Jung, E. H.; Jeon, N. J.; Park, E. Y.; Moon, C. S.; Shin, T. J.; Yang, T.-Y.; Noh, J. H.; Seo, J. Efficient, Stable and Scalable Perovskite Solar Cells Using Poly(3-Hexylthiophene). *Nature* **2019**, *567*, 511–515. https://doi.org/10.1038/s41586-019-1036-3.

(77) Sadhanala, A.; Yang, W.; Tu, Y.; Wang, Z.; Trindade, G. F.; Shivanna, R.; Chen, K.; Hu, Q.; Watts, J. F.; Zhang, Y.; et al. Enhanced Photovoltage for Inverted Planar Heterojunction Perovskite Solar Cells. *Science* **2018**, *360* (6396), 1442–1446. https://doi.org/10.1126/science.aap9282.

(78) Wang, Y.; Zhang, T.; Kan, M.; Zhao, Y. Bifunctional Stabilization of All-Inorganic A-CsPbI3 Perovskite for 17% Efficiency Photovoltaics. *Journal of the American Chemical Society* **2018**, *140*, 12345–12348. https://doi.org/10.1021/jacs.8b07927.

(79) Puurunen, R. L. Correlation between the Growth-per-Cycle and the Surface Hydroxyl Group Concentration in the Atomic Layer Deposition of Aluminum Oxide from Trimethylaluminum and Water. *Applied Surface Science* **2005**, *245* (1–4), 6–10. https://doi.org/10.1016/j.apsusc.2004.10.003.

(80) Elliott, S. D.; Greer, J. C. Simulating the Atomic Layer Deposition of Alumina from First Principles. *Journal of Materials Chemistry* **2004**, *14* (21), 3246–3250. https://doi.org/10.1039/b405776g.

(81) Hossain, M. A.; Khoo, K. T.; Cui, X.; Poduval, G. K.; Zhang, T.; Li, X.; Li, W. M.; Hoex, B. Atomic Layer Deposition Enabling Higher Efficiency Solar Cells: A Review. *Nano Materials Science* **2020**, *2*, 204–226. https://doi.org/10.1016/j.nanoms.2019.10.001.

(82) Abate, A.; Leijtens, T.; Pathak, S.; Teuscher, J.; Avolio, R.; Errico, M. E.; Kirkpatrik, J.; Ball, J. M.; Docampo, P.; McPherson, I.; et al. Lithium Salts as "Redox Active" p-Type Dopants for Organic Semiconductors and Their Impact in Solid-State Dye-Sensitized Solar Cells. *Physical Chemistry Chemical Physics* **2013**, *15* (7), 2572–2579. https://doi.org/10.1039/c2cp44397j.

(83) Schloemer, T. H.; Christians, J. A.; Luther, J. M.; Sellinger, A. Doping Strategies for Small Molecule Organic Hole-Transport Materials: Impacts on Perovskite Solar Cell Performance and Stability. *Chemical Science* **2019**, *10* (7), 1904–1935. https://doi.org/10.1039/C8SC05284K.

(84) Rainò, G.; Landuyt, A.; Krieg, F.; Bernasconi, C.; Ochsenbein, S. T.; Dirin, D. N.; Bodnarchuk, M. I.; Kovalenko, M. V. Underestimated Effect of a Polymer Matrix on the Light Emission of Single CsPbBr3 Nanocrystals. *Nano Letters* **2019**, *19* (6), 3648–3653. https://doi.org/10.1021/acs.nanolett.9b00689.

(85) Garner, L. E.; Nellissery Viswanathan, V.; Arias, D. H.; Brook, C. P.; Christensen, S. T.; Ferguson, A. J.; Kopidakis, N.; Larson, B. W.; Owczarczyk, Z. R.; Pfeilsticker, J. R.; et al. Photobleaching Dynamics in Small Molecule: Vs. Polymer Organic Photovoltaic Blends with 1,7-Bis-Trifluoromethylfullerene. *Journal of Materials Chemistry A* **2018**, *6* (11), 4623–4628. https://doi.org/10.1039/c7ta10995d.

(86) Seah, M. P.; Gilmore, I. S.; Beamson, G. XPS: Binding Energy Calibration of Electron Spectrometers 5 - Re-Evaluation of the Reference Energies. *Surface and Interface Analysis* **1998**, *26* (9), 642–649. https://doi.org/10.1002/(SICI)1096-9918(199808)26:9<642::AID-SIA408>3.0.CO;2-3.

(87) Harvey, S. P.; Zhang, F.; Palmstrom, A.; Luther, J. M.; Zhu, K.; Berry, J. J. Mitigating Measurement Artifacts in TOF-SIMS Analysis of Perovskite Solar Cells. *ACS Applied Materials and Interfaces* **2019**, *11* (34), 30911–30918. https://doi.org/10.1021/acsami.9b09445.

(88) Harvey, S. P.; Li, Z.; Christians, J. A.; Zhu, K.; Luther, J. M.; Berry, J. J. Probing Perovskite Inhomogeneity beyond the Surface: TOF-SIMS Analysis of Halide Perovskite Photovoltaic Devices. *ACS Applied Materials and Interfaces* **2018**, *10* (34), 28541–28552. https://doi.org/10.1021/acsami.8b07937.

(89) Harvey, S. P.; Messinger, J.; Zhu, K.; Luther, J. M.; Berry, J. J. Investigating the Effects of Chemical Gradients on Performance and Reliability within Perovskite Solar Cells with TOF-SIMS. *Advanced Energy Materials* **2020**, *10*, 1903674. https://doi.org/10.1002/aenm.201903674.

TOC graphic